Continuous Human Motion Recognition With a Dynamic Range-Doppler Trajectory Method Based on FMCW Radar

Chuanwei Ding, *Student Member, IEEE*, Hong Hong, *Member, IEEE*, Yu Zou, *Student Member, IEEE*, Hui Chu, Xiaohua Zhu, *Member, IEEE*, Francesco Fioranelli, *Member, IEEE*, Julien Le Kernec, *Senior Member, IEEE,* and Changzhi Li, *Senior Member, IEEE*

***Abstract*— Radar-based human motion recognition is crucial for many applications, such as surveillance, search and rescue operations, smart homes, and assisted living. Continuous human motion recognition in real-living environment is necessary for practical deployment, i.e., classification of a sequence of activities transitioning one into another, rather than individual activities. In this paper, a novel dynamic range-Doppler trajectory (DRDT) method based on the frequency-modulated continuous-wave (FMCW) radar system is proposed to recognize continuous human motions with various conditions emulating real-living environment. This method can separate continuous motions and process them as single events. First, range-Doppler frames consisting of a series of range-Doppler maps are obtained from the backscattered signals. Next, the DRDT is extracted from these frames to monitor human motions in time, range, and Doppler domains in real time. Then, a peak search method is applied to locate and separate each human motion from the DRDT map. Finally, range, Doppler, radar cross section (RCS), and dispersion features are extracted and combined in a multidomain fusion approach as inputs to a machine learning classifier. This achieves accurate and robust recognition even in various conditions of distance, view angle, direction, and individual diversity. Extensive experiments have been conducted to show its feasibility and superiority by obtaining an average accuracy of 91.9% on continuous classification.**

***Index Terms*— Continuous human motion recognition, dynamic range-Doppler trajectory (DRDT) method, frequency-modulated continuous-wave (FMCW) radar, fusion of multidomain features, machine learning.**

Manuscript received December 21, 2018; revised March 19, 2019; accepted March 25, 2019. This work was supported in part by the National Natural Science Foundation of China under Grant 61871224 and Grant 81601568, in part by the Key Research and Development Plan of Jiangsu Province under Grant BE2018729, in part by the Fundamental Research Funds for the Central Universities under Grant 30917011316, the State Scholarship Fund of the China Scholarship Council under Grant 201806840055, and in part by the National Science Foundation (NSF) under Grant ECCS-1808613 and Grant CNS-1718483. The work of F. Fioranelli was supported by U.K. Engineering and Physical Sciences Research Council under Grant INSHEP EP/R041679/1. *(Corresponding author: Hong Hong.)*

C. Ding is with the School of Electronic and Optical Engineering, Nanjing University of Science and Technology, Nanjing 210094, China, and also with the Department of Electrical and Computer Engineering, Texas Tech University, Lubbock, TX 79409 USA.

H. Hong, Y. Zou, H. Chu, and X. Zhu are with the School of Electronic and Optical Engineering, Nanjing University of Science and Technology, Nanjing 210094, China (e-mail: hongnju@njust.edu.cn).

F. Fioranelli is with the Communication, Sensing and Imaging Group, School of Engineering, University of Glasgow, Glasgow G128QQ, U.K. (e-mail: francesco.fioranelli@glasgow.ac.uk).

J. L. Kernec is with the Communication, Sensing and Imaging Group, School of Engineering, University of Glasgow, Glasgow G128QQ, U.K., also with the School of Information and Communications, University of Electronic Science and Technology of China, Chengdu 610000, China, and also with the Image and Signal Processing Laboratory, University of Cergy-Pontoise, 95011 Cergy, France (e-mail: julien.lekernec@glasgow.ac.uk).

C. Li is with the Department of Electrical and Computer Engineering, Texas Tech University, Lubbock, TX 79409 USA (e-mail: changzhi.li@ttu.edu).

Color versions of one or more of the figures in this paper are available online at http://ieeexplore.ieee.org.

Digital Object Identifier 10.1109/TGRS.2019.2908758

I. Introduction

HUMAN motion recognition has attracted great interest for different purposes, such as surveillance, search and rescue operations, smart home, and senior people care in assisted living facilities [1]–[5]. Various methods for human motion recognition have been proposed [6]–[9]. The employed sensors can be categorized into wearable and contactless solutions. Wearable sensors, such as bracelets and ankle monitors, must be worn or carried constantly, and thus are inconvenient, may be easily broken or forgotten, and have high false alarm rates [10]. Given these limitations, contactless detection technologies have gained wide research interests. The most common contactless sensors include cameras [8], microphones [9], and radar systems. Cameras are vulnerable to lighting conditions and blind spots. Microphones are sensitive to ambient noise interferes. Furthermore, they both infringe privacy issues, especially when deployed in private homes.

Radar-based human motion recognition may complement the conventional technologies because of its potential for high accuracy, robustness, and privacy preservation [11]. Typically, micro-Doppler features are utilized to detect, identify, and recognize human beings and their motions [12]–[17]. For example, Vandersmissen *et al.* [12] investigated micro-Doppler features from gait to identify five indoor persons with a classification error rate of 21.54%. Kim and Ling [13] utilized a continuous-wave (CW) radar to extract Doppler features for a support vector machine (SVM) classifier to recognize seven human motions. The accuracy of the classification results was 92.8%. Based on the rapid development of low-cost frequency-modulated continuous-wave (FMCW), stepped-frequency continuous wave (SFCW), and ultrawideband (UWB) radar, range and other information are involved [18]–[26]. A multidimensional principal component

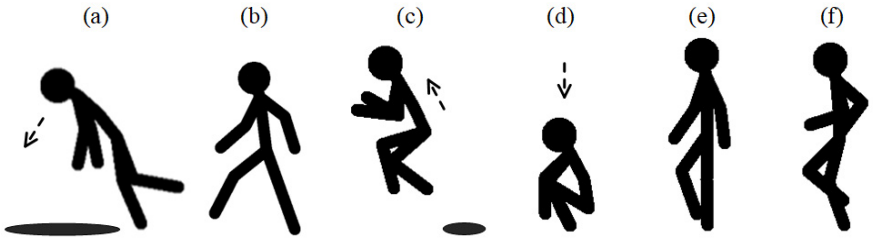

Fig. 1. Illustration of six typical human motions. (a) Falling. (b) Stepping. (c) Jumping. (d) Squatting. (e) Walking. (f) Jogging.

analysis (MPCA) was proposed to combine time, Doppler, and range information to improve fall detection based on an FMCW radar system [18]. An SFCW radar was used to extract phase information contained in the complex high-resolution range profile (HRRP) to derive instantaneous velocity, acceleration, and jerk of human body for fall detection and monitoring [19]. Radar cross section (RCS) information was also used to distinguish fall and other abrupt movements [20]. Bryan *et al.* [21] applied PCA in feature extraction to classify eight human activities based on UWB radar and achieved a recognition accuracy of over 85%. Recently, deep learning methods emerged as an effective tool in human motion recognition using different radar systems [27]–[30].

However, most studies focused on motion recognition in a laboratory environment, whereby the different activities are recorded as separate and individual snapshots. Practical applications would need to deal with continuous human motion recognition in real-living conditions, where the human subject monitored can perform activities one after another with unknown durations and transitions in between.

In this paper, a novel method is proposed to explore and demonstrate its feasibility and performance from snapshot motion recognition to continuous motion recognition with various conditions from real-living environments. A novel dynamic range-Doppler trajectory (DRDT) method is introduced to obtain DRDT map from backscattered radar signals, which can help monitor human motions in range, Doppler, and RCS domains in real time. This makes it possible to apply a peak search method to initially locate and separate the contributions of each individual activity in a continuous recording, and then process them as single events. In addition, not only the commonly used micro-Doppler features but also time-varying features in radar multidomains are extracted as inputs to machine learning classifiers in a multidomain perspective. This leads to accuracy and robust recognition performance even in various conditions of distance, view angle, direction, and individual diversity.

The rest of this paper is organized as follows. Section II introduces the theory and algorithm of the DRDT method. In Section III, the FMCW radar system and experimental setup are described. Section IV presents analysis and discussion of the recognition results. Section V is the conclusion.

II. Theory and Algorithm

In daily life, falling is among the leading causes of fatal and nonfatal injuries, especially for senior people [31]. Therefore, falling and its similar human activities are selected for recognition in this paper. These include *falling*, *stepping*, *jumping*, *squatting*, *walking,* and *jogging*. An illustration of these human motions is shown in Fig. 1, and the detailed descriptions are given in Table I. In order to recognize these human motions in a real-living environment, a novel DRDT, DRDT method, is proposed.

TABLE I
Six Human Motions Under Study

Motions	Description
Falling	Drop forward to the floor under the influence of gravity.
Stepping	Abrupt movement toward radar.
Jumping	Jumping forward with swinging arms and legs.
Squatting	Sitting in a crouching position with knees bent.
Walking	Walking forward at a moderate speed while swinging arms.
Jogging	Running at a gentle pace with fist at the height of chest

This approach can be divided into five steps summarized here and detailed in Sections II-A–II-E. First, by processing the backscattered radar signals, a series of range-Doppler maps called range-Doppler frames can be obtained with given time windows [20], as detailed in Section II-A. Section II-B explains how the DRDT is extracted from the above frames to describe human motion in time, range, Doppler, and RCS domains. Section II-C then describes how a single motion is identified and separated from a series of continuous activities with a peak search method. Section II-D shows how the features in multiple domains are extracted based on the DRDT map. Finally, Section II-E introduces the subspace K-nearest neighbor (KNN) classifier [32] used to obtain the final recognition results.

A. Conventional Range-Doppler Frames

The received signals can be rearranged in a matrix, whose rows represent the slow time and columns contain the received signals in fast time. By performing an FFT along the fast time, the signals are discretized and the values are stored in an $N \times M$ matrix $R(n, m)$. $n = [1, 2, \ldots, N]$ indicates the index of slow time and $m = [1, 2, \ldots, M]$ indicates the index of the beat frequency corresponding to range bins. Then, a range-Doppler map can be obtained by performing an FFT along the slow time direction with a sliding time window. To obtain time-varying range-Doppler information, i.e., a continuous sequence of range-Doppler frames over time, a single range-Doppler frame can be achieved by setting a time

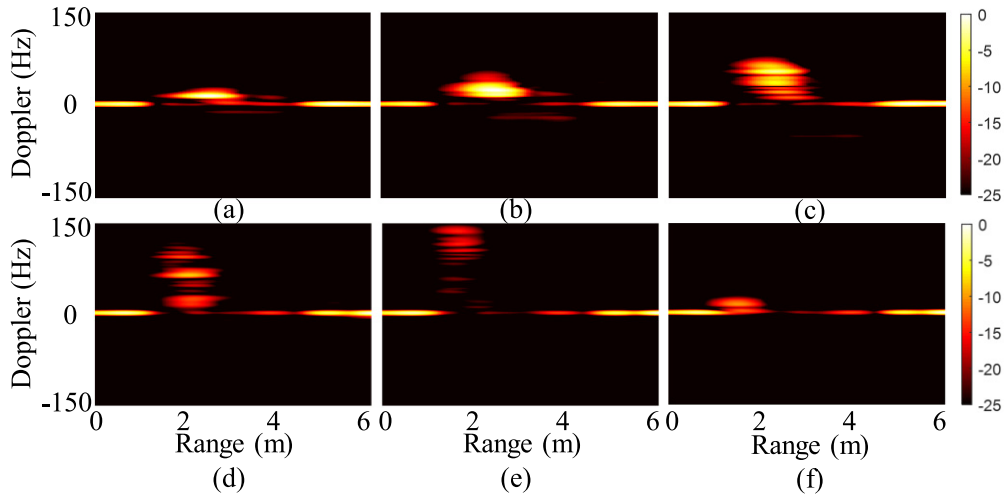

Fig. 2. Conventional range-Doppler frames. (a)–(f) Six range-Doppler frames of falling toward the radar.

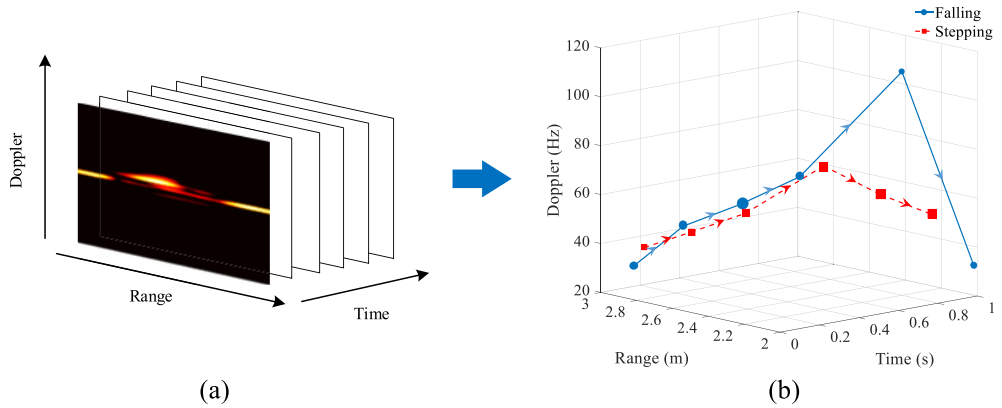

Fig. 3. Illustration of DRDT processing. (a) Conventional range-Doppler frames. (b) DRDT of *falling* and *stepping*.

window with limited duration

$$F(k,m)=\sum_{n=1}^{L}R(n,m)e^{-j2\pi nk/L} \tag{1}$$

where k indicates the index of frequency and L is the length of the time window, which corresponds to 0.2-s time duration of each range-Doppler frame.

B. Proposed Dynamic Range-Doppler Trajectory

DRDT is utilized to describe and monitor human motions in range, Doppler, and RCS domains in real time. This is obtained by extracting key information from conventional range-Doppler frames. One frame corresponds to one point in a DRDT map.

P frames are selected as effective frames to describe an entire human motion denoted as $F_p(k,m)$, $p\in[1,P]$. In this paper, the value of P is set to 6, corresponding to 1.2 s. There is a tradeoff on the number of frames in order to cover an entire human action while avoiding the inclusion of too many uninformative frames. The value of P was empirically verified through observations of the most common human motions. Fig. 2 shows an example of six range-Doppler frames for *falling*. Each frame indicates range, Doppler, and RCS information of human body during falling motion.

Since the other motions may have high Doppler components similar to the case of *falling*, the baseband signals close to 0 Hz are initially removed by an empirical Doppler threshold corresponding to a velocity of 0.45 m/s in each range-Doppler frame. Next, the top Q points in energy, i.e., those related to high RCS, are selected as points of interest denoted as $F_p(k_{pq},m_{pq})$, where $q=[1,2,\ldots,Q]$ indicates the index of the points of interest. Then, the weighted average for the points of interest is calculated to constitute a DRDT map.

Fig. 3 shows the process of extracting typical DRDT maps of *falling* and *stepping*. Every trajectory point in the DRDT map represents one dynamic range-Doppler frame. Its coordinates are obtained as shown in (2) and (3) in the corresponding frame, and its size in Fig. 3 indicates the energy calculated with (4)

$$E_{pq}=F_p(k_{pq},m_{pq})^2,\sigma_{pq}=E_{pq}/\sum_{q=1}^{Q}E_{pq} \tag{2}$$

$$(k_p,m_p)=\sum_{q=1}^{Q}\sigma_{pq}(k_{pq},m_{pq}) \tag{3}$$

$$E_p=\frac{1}{Q}\sum_{q=1}^{Q}E_{pq} \tag{4}$$

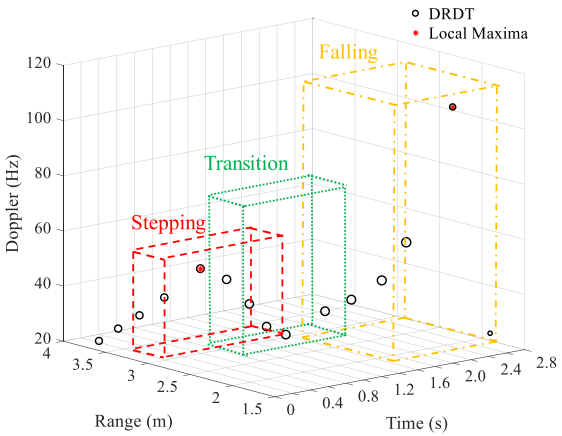

Fig. 4. Two continuous motions of *stepping* → *falling* in DRDT map.

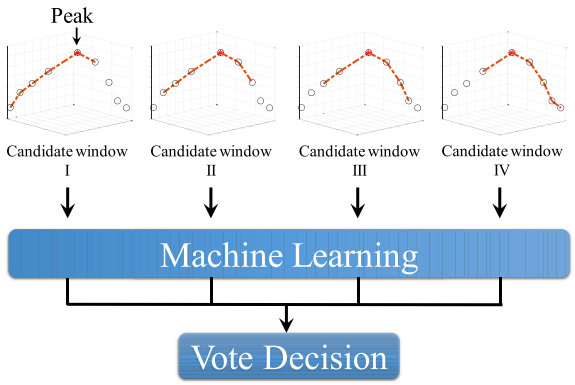

Fig. 5. Diagram of the proposed peak search method.

where $F_p(k_{pq}, m_{pq})$ is the qth point of interest in the pth frame, E_{pq} represents its energy, σ_{pq} is the weighted coefficient defined according to E_{pq}, (k_{pq}, m_{pq}) is the Doppler and range coordinates of the DRDT, and E_p is its corresponding energy.

As shown in Fig. 3(b), the blue circles indicate the trajectory of *falling*, while the red rectangles represent *stepping*. Their sizes represent the energy level relating to the target RCS information of each frame. At the beginning of the *falling* motion, the trajectory rises up slowly and smoothly along with a decreasing distance and increasing Doppler and energy. Then, it reaches a sudden high peak. The peak has the maximum Doppler for the highest radial velocity, while its energy decreases sharply due to the lowest RCS caused by the orientation of the body on the floor and being at an angle from the center of the radar beam. On the other hand, red rectangles represent *stepping*. It shows a similar trend in the range and Doppler domains with a lower maximum Doppler and range span. However, the RCS of human body does not change much during *stepping*, which is different from *falling*.

C. Continuous Motion Recognition

In real-living environments and conditions, continuous motion recognition is a challenging task, as accurately locating and separating each activity in a long period of time is not trivial. One needs to characterize not only each individual activity but also the transitions between them and their duration. Fig. 4 shows the two continuous motions of *stepping* followed by *falling* in the proposed DRDT map. The black circles indicate DRDT. It is obvious that besides *stepping* (red window) and *falling* (yellow window) samples, there are a lot of transition samples which by themselves do not belong to any meaningful motion labels, highlighted by the green window in Fig. 4. They are called and labeled as *transition*. A classic approach would be to use a sliding window method to extract each time sequence of length P as a sample for feature extraction and machine learning. However, a large amount of *transition* samples can be observed with the sliding window method, and this may lead to complex calculations and instability. The key point of continuous motion recognition is to locate meaningful single motions and remove transitions as much as possible.

In this paper, a peak search method based on DRDT is proposed to address this problem. Since all the motions of interest in the application have high Doppler components, these can be characterized by a peak in DRDT maps. Therefore, a peak search is applied to locate and extract samples containing local maxima, which may correspond to meaningful motion labels. Different from the standard peak search method, only the trajectory points whose Doppler frequency is larger than both its former and later two points, i.e., (k_{p^*}, m_{p^*}), $k_{p^*} \geq k_p$, $p \in [p^* - 2, p^* + 2]$, can be selected as local maxima. The choice of $+/-$ two points is a tradeoff between leakage alarm rate and false alarm rate, which was adjusted empirically to maximize performance.

Fig. 5 shows the diagram of the proposed peak search method. The red asterisks in both Figs. 4 and 5 indicate local maxima extracted by the peak search method. As mentioned in Section II-A, each motion is assumed to occupy six frames, i.e., a six-point window in the DRDT map. This means that once the peak is identified, the most appropriate six-point window should be selected as an effective set of data representing the activity to be classified, rather than the transitions. However, due to the variability of motions and differences in the signatures even for the same motion, the peak may be located at any position in the most appropriate window, except for the beginning and the end. Therefore, among the six candidate windows, the four with their peaks located at the second, third, fourth, and fifth positions, respectively, are selected to be passed to the feature extraction and classification stage. As shown in Fig. 5, four candidate trajectories of a stepping motion were selected and represented by red dashed lines after the peak was located. Then, features extracted from these four trajectories were fed into the machine learning classifier to obtain their independent recognition result. Finally, a vote decision was conducted with these results based on the principle of minority obeying majority. In particular, only when there are four recognition results for *transition*, the final decision is labeled as *transition*. Otherwise, the motion labels are combined with majority voting and the transition is disregarded. Furthermore, if there is a situation of a tie between two meaningful motion labels, which rarely happens, the former meaningful motion is chosen as the final decision.

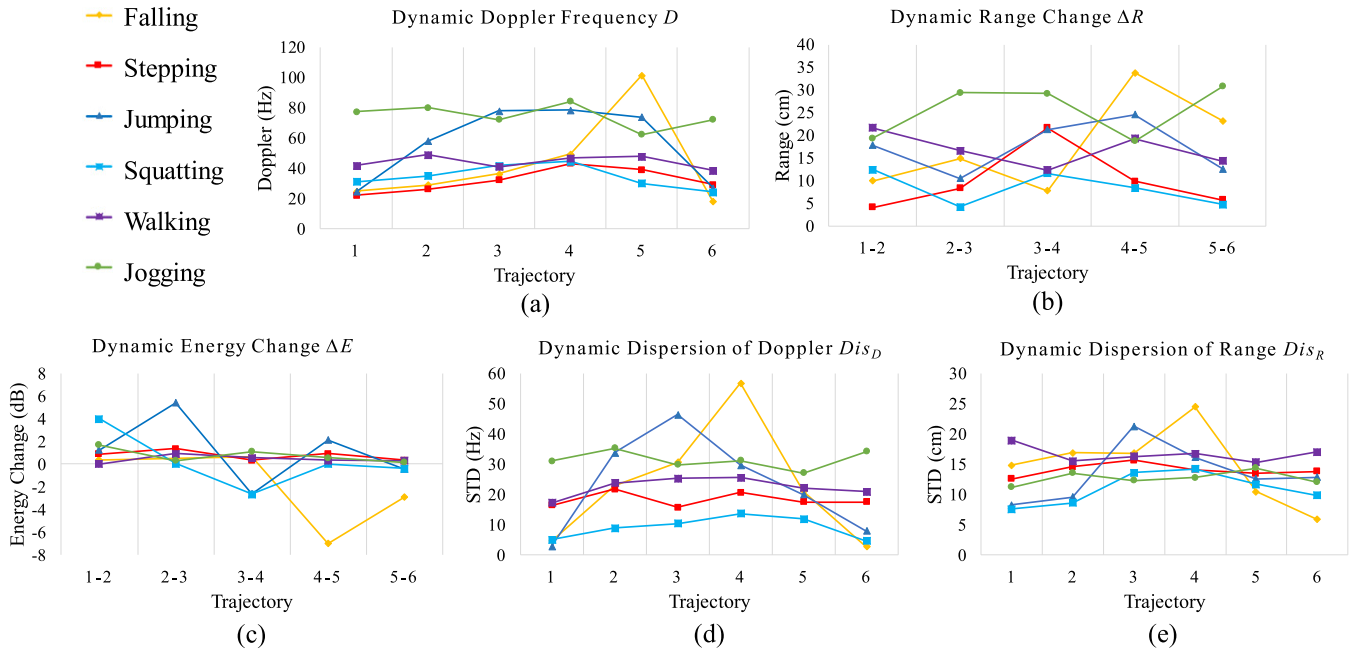

Fig. 6. Features extracted from typical examples of six human motions. (a) Dynamic Doppler frequency D. (b) Dynamic range change ΔR. (c) Dynamic energy change ΔE. (d) and (e) Dynamic dispersion of Doppler and range Dis_D and Dis_R.

D. Feature Extraction

In feature extraction, a comprehensive fusion of time, range, Doppler, RCS, and dispersion features is applied; 28 features of four types are extracted based on DRDT maps as follows.

1) Dynamic Doppler Frequency—D: This feature consists of a time sequence of the Doppler value along the trajectory. It represents the time-varying intensity of human motions

$$D(p) = k_p \tag{5}$$

Fig. 6(a) shows the dynamic Doppler frequency D of each motion in DRDT maps. Note that as an abrupt motion, *falling* is characterized with a high and rapid Doppler peak, while *jumping* has a stable up and down trend. The dynamic Doppler frequency features of *jogging* are generally higher than the ones of *walking* although they have similar trajectory trends. It is difficult to distinguish between *stepping* and *squatting* only with Doppler features.

2) Dynamic Range Change ΔR: Range information is crucial for human motion recognition. Fusion of range and time is considered with a time sequence of range coordinates. Furthermore, for situations of different detection distances, it is adjusted as a time sequence of relative range change. This feature describes the relative range change during human motion and, to some degree, indicates motion velocity and range span

$$\Delta R(i) = m_{i+1} - m_i, \quad i \in [1, P-1]. \tag{6}$$

As shown in Fig. 6(b), all motions in the figure are performed moving toward the radar because of positive values of ΔR. In addition, a rapid increase of range can be found during the *falling*. *Walking* and *jogging* both have a stable increase in range and the latter has a faster velocity. In this figure, *stepping* can be distinguished from *squatting* for its larger range span and peak in the middle of the trajectory.

3) Dynamic Energy Change—Δ E: Considering the effects of distance, this feature is based on the time-dependent energy change. It indicates the time-varying RCS, which is important to discriminate motions that are similar in range and Doppler, e.g., *falling* and *jumping* or fast *stepping*

$$\Delta E(i) = E_{i+1} - E_i, \quad i \in [1, P-1]. \tag{7}$$

Fig. 6(c) describes the dynamic energy change ΔE of six typical motions. As *falling* happens, its energy increases at first when the body approaches the radar. Then, it drops rapidly to the minimum due to the orientation of the body deviating from the center of the radar beam. On the other hand, during *jumping*, the takeoff part contributes to a high positive dynamic energy change at first. Then, the following half-squat landing leads to a negative energy change. The last straightening up causes a positive change again. Other motions always have a positive energy change for approaching the radar, but there is a negative one in *squatting*, as the human subject leaves the center of the radar beam.

4) Dynamic Dispersion of Range and Doppler Dis_D and Dis_R: These features are obtained from the standard deviation (STD) of range and Doppler coordinates for the points of interest. Two time sequences of range and Doppler STD reflect features of limb movement. A large STD corresponds to a large amplitude limb movement

$$\begin{cases} \mathrm{Dis}_D(p) = \mathrm{STD}(k_{pq}) \\ \mathrm{Dis}_R(p) = \mathrm{STD}(m_{pq}). \end{cases} \tag{8}$$

Fig. 6(d) and (e) shows the dynamic dispersion of Doppler and range, respectively. There exists spontaneous swinging arm during *falling*, which contributes to large Dis_D and Dis_R. It is the same in *jumping*. In addition, Dis_D of *jogging* is higher than that of *walking*, while the contrary occurs in the

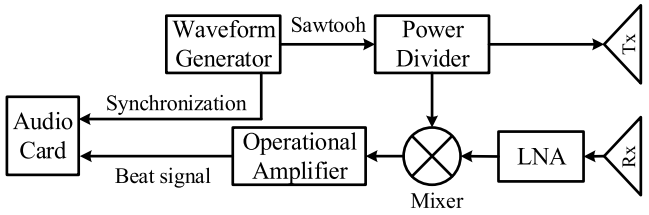

Fig. 7. Block diagram of the FMCW radar system.

TABLE II
KEY PARAMETERS OF THE FMCW RADAR SYSTEM

Center frequency	5.8GHz
Transmitted bandwidth	320MHz
Sampling frequency	44.1KHz
Frequency ramp repetition period	10ms
Average transmitted power	8dBm

case of Dis_R caused by the difference between putting fists on the chest and swinging arms.

E. Machine Learning

In statistics and machine learning, ensemble methods use multiple learning algorithms to obtain better classification performance [33]. Unlike a statistical ensemble in statistical mechanics, which is usually infinite, a machine learning ensemble refers only to a concrete finite set of alternative models, but it typically allows for much more flexible structure to exist among those alternatives. After comparing each ensemble classifier, subspace KNN is adopted to analyze the above features based on the Classification Learner Tool in MATLAB R2016b.

III. EXPERIMENTAL SETUP

The block diagram of the FMCW radar system used in this paper is shown in Fig. 7 [34]. A pair of 2×2 patch antenna arrays are used to transmit and receive C-band signals. The waveform generator generates a linear chirp signal around 5.8 GHz, which is fed to the power divider with a baseband synchronization signal locked to the sawtooth oscillator control signal. The coherence of the system is achieved by simultaneously sampling the beat signal from the receiver output and the synchronization signal from the waveform generator. A data acquisition interface is employed to digitize the baseband output through the audio card of a laptop, facilitating real-time signal processing in the laptop. The key parameters of the radar system are listed in Table II.

The experimental setup is shown in Fig. 8. The radar system was set at a height of 1 m. Six typical human motions were selected in this paper, as shown in Fig. 1 and detailed in Table I. Eight volunteers, including five males and three females, were enrolled in this paper. Table III gives a brief physical description of the volunteers. Their ages ranged from 23 to 28 years and weights ranged from 50 to 85 kgs, with height from 1.58 to 1.80 m.

In the first scenario, the volunteers performed single human motion in indoor environment under the line-of-sight condition. However, practical human motion recognition

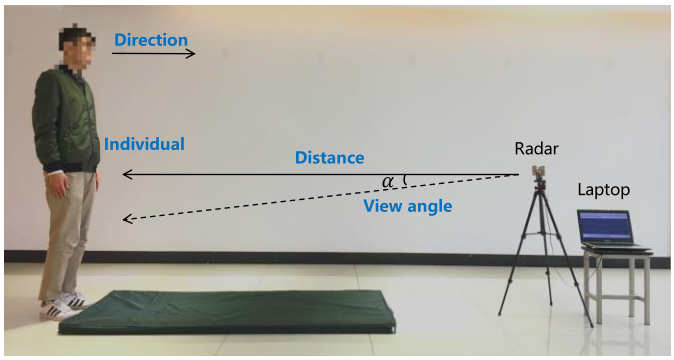

Fig. 8. Experimental Setup.

TABLE III
BRIEF PHYSICAL DESCRIPTION OF THE VOLUNTEERS

Volunteers	Gender	Age (yr)	Weight (kg)	Height (m)	BMI (kg/m^2)
1	M	23	85	1.75	27.76
2	M	28	78	1.80	24.07
3	M	24	72	1.79	22.47
4	M	25	70	1.77	22.34
5	M	23	68	1.80	20.99
6	F	24	50	1.58	20.03
7	F	23	55	1.62	20.96
8	F	25	64	1.68	22.68
Total	M/F (5/3)	24.4±1.7	67.8±11.4	1.72±0.09	22.66±2.41

in real-living environment may face additional challenges, such as variations in distance, view angle, movement direction, and individual characteristics. To evaluate their effects on the proposed method, eight volunteers performed six motions toward the radar at 2∼3 m with the view angle of 0° as a reference group. Then, experiments with different conditions were recorded as validation groups. Detailed illustrations and descriptions are provided in Table IV. In each condition, eight volunteers performed each motion for five times to obtain a total of 240 measurements.

In the second scenario, unlike separate and individual snapshots, the volunteers performed any two of the aforementioned motions continuously, one after the other, to evaluate motion recognition performance of the proposed method. For this purpose, ten combinations were selected to cover as many practical situations as possible, including: *walking* → *falling*, *stepping* → *falling*, *jogging* → *falling*, *jumping* → *falling*, *walking* → *jumping*, *walking* → *stepping*, *jogging* → *squatting*, *stepping* → *squatting*, *jumping* → *stepping*, *jumping* → *squatting*. Each combination was performed 15 times with two volunteers.

IV. RESULTS

To evaluate the feasibility and performance of the proposed method in human motion recognition, two tests were performed, i.e., single motion recognition and continuous motion recognition. In Section IV-A, the results for single motion recognition are analyzed to demonstrate human

TABLE IV
ILLUSTRATION AND DESCRIPTION OF EXPERIMENTS IN VARIOUS CONDITIONS

Variations	Illustration	Description
Distance	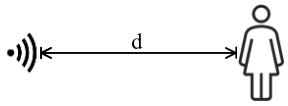	Volunteers perform each motion at the different distance of d (d=2 ~ 4m)
View angle	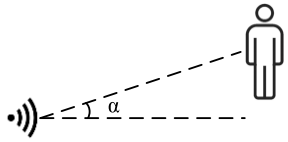	Volunteers perform each motion at the different view angle of $\alpha\left(\alpha=0^{\circ},15^{\circ},30^{\circ}\right)$
Direction	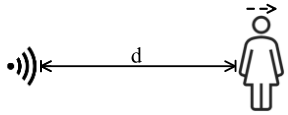	Volunteers perform each motion with the different direction (towards and backwards radar)
Individual	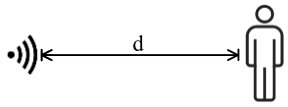	Different volunteers perform each motion in above situations

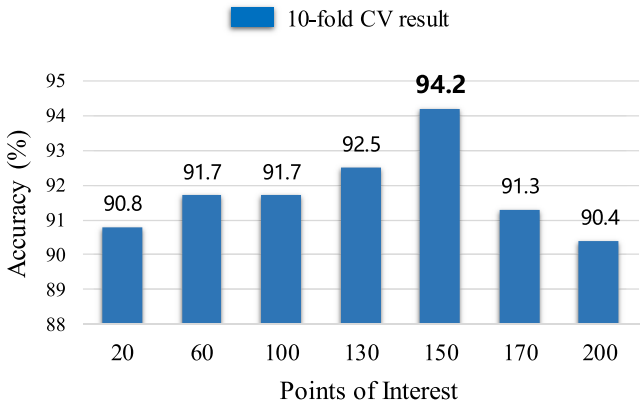

Fig. 9. Classification accuracy with a different number of points from a range-Doppler frame.

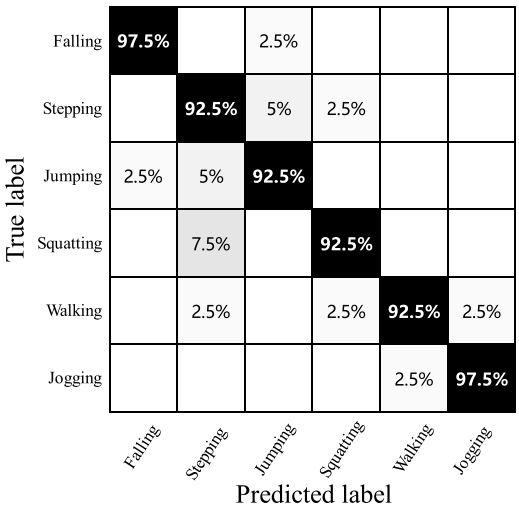

Fig. 10. Confusion matrix of single motion recognition.

motion recognition performance of the DRDT method with different distances, view angles, directions, and individuals. In Section IV-B, recognition results demonstrate the good

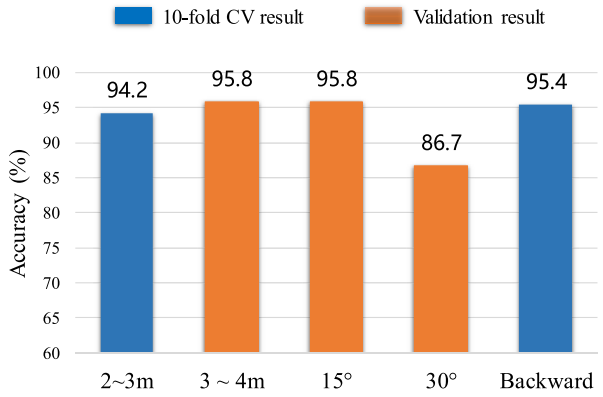

Fig. 11. Classification accuracy in different scenarios.

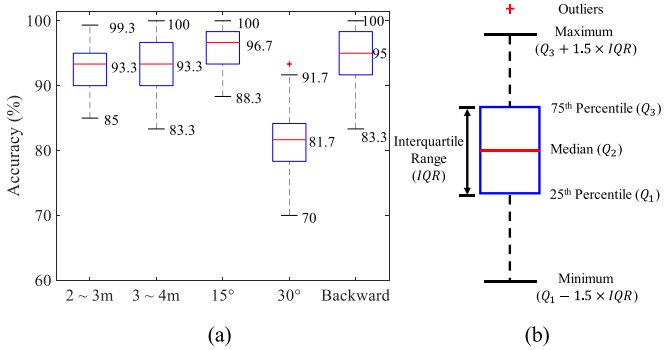

Fig. 12. Boxplot of recognition accuracy in individual diversity study. (a) Recognition accuracy in different conditions. (b) Legend of boxplot

performance of the proposed DRDT method for continuous motion recognition.

A. Single Motion Recognition

First, volunteers performed the six motions toward the radar at the distance of 2∼3 m with the view angle of 0° as a basic experiment (*walking* and *jogging* were performed in a range scope of 2∼4 m). To confirm the optimal value of Q,

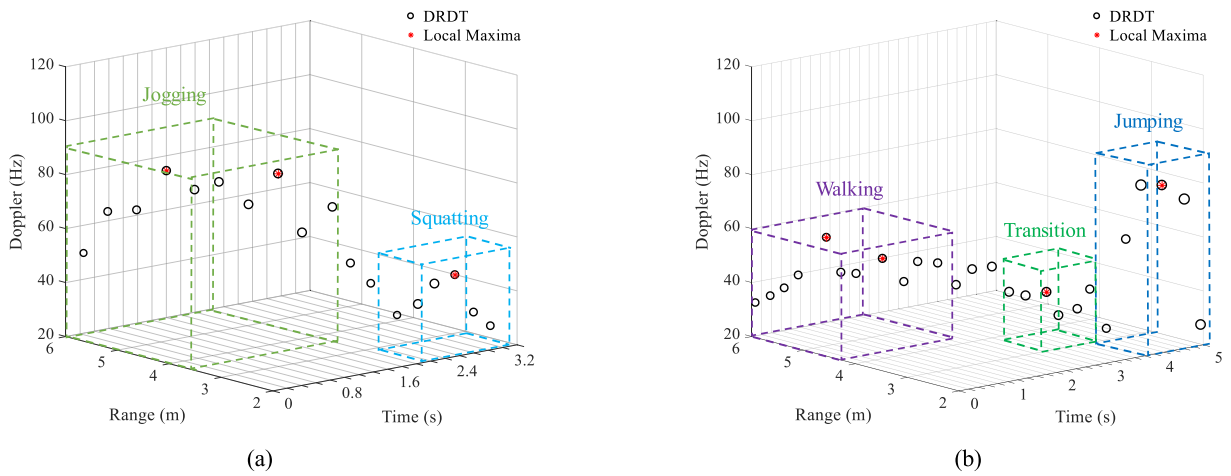

Fig. 13. Typical examples of two continuous motions in DRDT map. (a) *Jogging* → *squatting*. (b) *Walking* → *jumping*.

the number of points to be extracted from each range-Doppler frame and the classification results with different selections of Q are compared. As shown in Fig. 9, when Q is set as 150, classification of all the six motions achieved the highest accuracy rate of 94.2%.

Fig. 10 shows the corresponding confusion matrix. It is shown that the proposed solution achieved a high classification accuracy for all human motions considered. In particular, *falling* and *jogging* obtained the highest level of classification accuracy of 97.5%. On the other hand, *squatting* had the lowest accuracy of 92.5%, as 7.5% of them were misclassified as *stepping*. This is conceivable—*squatting* forward with high amplitude is similar to a slow *stepping*.

To evaluate the robustness of the proposed method at different target distances, 240 measurements with the same eight volunteers and the same experimental setup but at 3∼4 m were conducted. This provided a validation data set to test the existing model trained by 2∼3-m data (*walking* and *jogging* were performed in a range scope of 2∼4 m). As shown in Fig. 11, an average validation accuracy rate of 95.8% was achieved because the adopted dynamic range change feature ΔR can decrease the influence of detection distance.

In addition, robustness for different view angles was also evaluated using 480 measurements at the degree of 15° and 30° to test the above model at 0°. As shown in Fig. 11, at a view angle of 15°, the classification accuracy rate was 95.8%, which is similar to the line-of-sight case. However, only 86.7% of motions were recognized correctly at 30°, as the target got too close to the edge of the main beam, resulting in a loss of useful information.

Regarding experiments with different directions, it is obvious to distinguish between backward motions and forward ones owing to the dynamic range change and Doppler features. Among 240 samples of backward motions, the DRDT method also achieved a high recognition accuracy of 95.4% with the tenfold CV procedure.

The effect of individual diversity on the proposed DRDT method is also investigated. Indeed, classifying human motions of unknown people based on trained data from known people is a realistic and practical situation. A leave-out technique

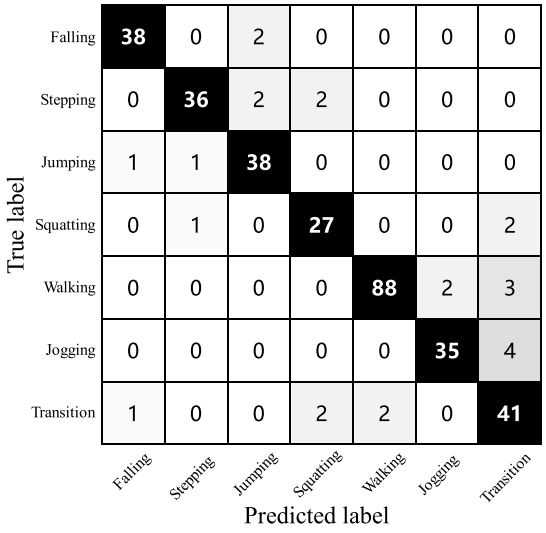

Fig. 14. Confusion matrix of two continuous motions' recognition.

is chosen to test the performance for the eight volunteers. The samples from seven individuals were used to train the algorithm and then it was tested on the person that was left out. In each different condition considered, each test with the eighth subject was repeated for 35 times to get a robust evaluation. Test results are shown as typical boxplot in Fig. 12. The boxplot indicates the distribution of the test accuracy rates in each condition. The upper and lower boundaries of the blue box represent the third and first quartiles of all the accuracy rates, which are denoted by Q_3 and Q_1, respectively. This means half of the test accuracy rates are located in the blue box. The size of the box, indicated by IQR, corresponds to its robustness. The red line in the box means the median value, which is denoted by Q_2. Points with values higher than $(Q_3 + 1.5 \times IQR)$ or lower than $(Q_1 - 1.5 \times IQR)$ are identified as outliers and marked by red crosses. As shown in Fig. 12, the test accuracy in each condition was distributed in a relatively small box (<6.67%), which means a small discrepancy for different individuals. In the experiment at 30°, although there was a large gap between the minimum test

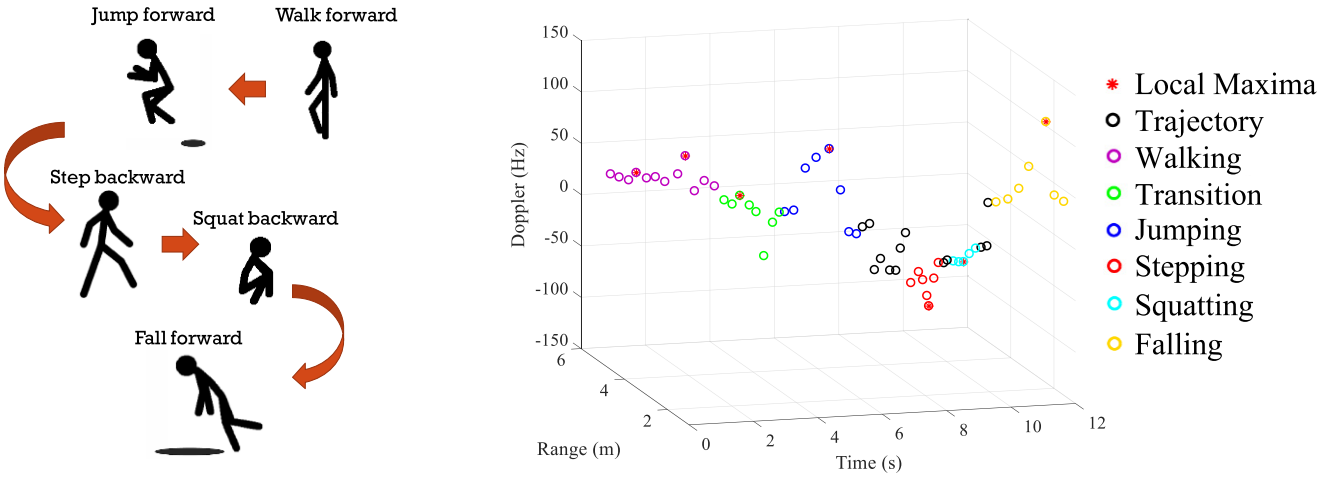

Fig. 15. Illustration and DRDT map of free-move motions.

accuracy of 70.0% and the maximum of 91.7%, most of them were distributed around the median accuracy of 81.7%. These results demonstrated the robust performance of the proposed DRDT method for different individuals.

B. Continuous Motion Recognition

In this section, continuous human motion recognition based on the DRDT method is evaluated. One-third of data was selected as a training group. Then, the peak search method was applied to extract samples of interest from the remaining data to test the training model.

Fig. 13 shows typical examples of two continuous motions in the DRDT map. As shown in Fig. 13(a), three local maxima, i.e., peaks marked as red asterisks were found during the measurement. The samples containing the first two peaks were recognized as *jogging*, while the remaining was *squatting*. *Jogging* is characterized with high and rhythmic Doppler, steady velocity, and large dispersion in both range and Doppler. The DRDT of *squatting* is similar to that of *stepping* but with a lower Doppler peak, weaker RCS, and smaller range span. Fig. 13(b) describes one combination of *walking* $\rightarrow$ *jumping*. The samples containing the first three peaks were classified as *walking*. Compared with *jogging* in Fig. 13(a), *walking* had a lower Doppler and velocity. The fourth peak represented the *transition* between *walking* and the following *jumping*, which was indicated by the last peak. Note that there were more labels obtained for *walking* and *jogging* in one measurement, which is reasonable as *walking* and *jogging* are usually performed continuously for a relatively long duration in practical situations.

Fig. 14 shows the confusion matrix of all the test results. The average recognition accuracy was 91.9%. In addition, *transition* instances could also be recognized with an accuracy of 89.1%. Furthermore, the number of labels, i.e., extracted peaks, of *falling*, *stepping*, *jumping*, and *squatting* was consistent with the ground truth. This indicated that the proposed peak search method can accurately extract samples of interest during these motions and reduce a large amount of calculation at the same time.

Furthermore, the performance of the proposed DRDT method in a more complex situation close to a completely uncontrolled environment was also investigated. The volunteer performed a series of motions in front of the radar at random distances with arbitrary view angles in all directions. An example corresponding DRDT map is shown in Fig. 15. As mentioned in Section II-C, the most appropriate windows were decided after a majority vote and marked in different colors according to the recognition results. From the figure, all motions of the volunteer can be monitored. At first, the volunteer walked toward the radar as indicated by the red circles. After a short pause, blue circles indicated that the subject began to jump toward the radar. Between these two motions, there was also a transition marked in green. Then, the subject turned back and took a step backward. The following motion can be recognized as *squatting*. Finally, the subject turned back, faced radar again, and fell down toward the radar.

V. Conclusion

Going further than typically studied single human activity recognition in a laboratory environment, this paper proposed a novel DRDT method for continuous human motion recognition in conditions emulating real-living environments, where the people monitored can perform activities one after the other with unknown duration and with transitions in between. With a peak search method, continuous human motions can be located and accurately separated during a long-time monitoring with little calculation. In addition, besides micro-Doppler, multidomain information, including time, range, Doppler, RCS, and dispersion, was utilized in feature extraction. Experiments in varying conditions achieved robust recognition accuracies reaching about 95%. The performance degraded with view angle at about 30°, which is reasonable as the target got too close to the edge of the radar bandwidth. Recognition of continuous motions also achieved good performance with an average accuracy of 91.9% which enabled free-motion recognition in a real-living environment.

As this is a preliminary investigation in continuous human motion recognition, there is a large scope of further work

in the future. First, data from senior human subjects will be obtained to expand the database. Algorithm will also be improved to use fewer empirical parameters and enable recognition of motions with small Doppler. In addition, a more realistic environment with clutters, such as animals or multi-human targets, should be considered as a great challenge for indoor human motion recognition. Furthermore, the feasibility of a real-time human motion recognition system will be explored.

REFERENCES

[1] S. Z. Gurbuz, U. Kaynak, B. Ozkan, O. C. Kocaman, F. Kiyici, and B. Tekeli, "Design study of a short-range airborne UAV radar for human monitoring," in *Proc. 48th Asilomar Conf. Signals, Syst., Comput.*, 2014, pp. 568–572.

[2] F. Fioranelli, M. Ritchie, and H. Griffiths, "Classification of unarmed/armed personnel using the NetRAD multistatic radar for micro-Doppler and singular value decomposition features," *IEEE Geosci. Remote Sens. Lett.*, vol. 12, no. 9, pp. 1933–1937, Sep. 2015.

[3] P. Khomchuk, I. Stainvas, and I. Bilik, "Pedestrian motion direction estimation using simulated automotive MIMO radar," *IEEE Trans. Aerosp. Electron. Syst.*, vol. 52, no. 3, pp. 1132–1145, Jun. 2016.

[4] H. F. Wang, L. Y. Ren, E. K. Mao, and A. E. Fathy, "Phase based motion characteristics measurement for fall detection by using stepped-frequency continuous wave radar," in *Proc. IEEE Topical Conf. Biomed. Wireless Technol., Netw., Sens. Syst. (Biowireless)*, Jan. 2016, pp. 43–45.

[5] P. H. Chen, M. C. Shastry, C. P. Lai, and R. M. Narayanan, "A portable real-time digital noise radar system for through-the-wall imaging," *IEEE Trans. Geosci. Remote Sens.*, vol. 50, no. 10, pp. 4123–4134, Oct. 2012.

[6] A. I. Cuesta-Vargas, A. Galán-Mercant, and J. M. Williams, "The use of inertial sensors system for human motion analysis," *Phys. Therapy Rev.*, vol. 15, no. 6, pp. 462–473, 2010.

[7] O. D. Lara and M. A. Labrador, "A survey on human activity recognition using wearable sensors," *IEEE Commun. Surveys Tuts.*, vol. 15, no. 3, pp. 1192–1209, Jul. 2013.

[8] E. Cippitelli, F. Fioranelli, E. Gambi, and S. Spinsante, "Radar and RGB-depth sensors for fall detection: A review," *IEEE Sensors J.*, vol. 17, no. 12, pp. 3585–3604, Jun. 2017.

[9] J. A. Ward, P. Lukowicz, G. Troster, and T. E. Starner, "Activity recognition of assembly tasks using body-worn microphones and accelerometers," *IEEE Trans. Pattern Anal. Mach. Intell.*, vol. 28, no. 10, pp. 1553–1567, Oct. 2006.

[10] M. G. Amin, Y. D. Zhang, F. Ahmad, and K. C. Ho, "Radar signal processing for elderly fall detection the future for in-home monitoring," *IEEE Signal Process. Mag.*, vol. 33, no. 2, pp. 71–80, Mar. 2016.

[11] M. G. Amin, *Through-the-Wall Radar Imaging*. Boca Raton, FL, USA: CRC Press, 2017.

[12] B. Vandersmissen *et al.*, "Indoor person identification using a low-power FMCW radar," *IEEE Trans. Geosci. Remote Sens.*, vol. 56, no. 7, pp. 3941–3952, Jul. 2018.

[13] Y. Kim and H. Ling, "Human activity classification based on micro-Doppler signatures using a support vector machine," *IEEE Trans. Geosci. Remote Sens.*, vol. 47, no. 5, pp. 1328–1337, May 2009.

[14] B. Tekeli, S. Z. Gürbüz, and M. Yuksel, "Information-theoretic feature selection for human micro-Doppler signature classification," *IEEE Trans. Geosci. Remote Sens.*, vol. 54, no. 5, pp. 2749–2762, May 2016.

[15] Y. Z. Wang, Q. H. Liu, and A. E. Fathy, "CW and pulse-Doppler radar processing based on FPGA for human sensing applications," *IEEE Trans. Geosci. Remote Sens.*, vol. 51, no. 5, pp. 3097–3107, May 2013.

[16] V. C. Chen, "Doppler signatures of radar backscattering from objects with micro-motions," *IET Signal Process.*, vol. 2, no. 3, pp. 291–300, Sep. 2008.

[17] B. Y. Su, K. C. Ho, M. J. Rantz, and M. Skubic, "Doppler radar fall activity detection using the wavelet transform," *IEEE Trans. Biomed. Eng.*, vol. 62, no. 3, pp. 865–875, Mar. 2015.

[18] B. Erol and M. G. Amin, "Radar data cube analysis for fall detection," in *Proc. IEEE Int. Conf. Acoust., Speech Signal Process. (ICASSP)*, 2018, pp. 2446–2450.

[19] N. Tran, O. Kilic, S. Nahar, L. Ren, H. Wang, and A. Fathy, "Contactless monitoring and classification of human motion activities by using SFCW radar," in *Proc. IEEE Antennas Propag. Soc. Int. Symp.*, Jun. 2016, pp. 883–884.

[20] Z. Y. Peng, J. M. Muñoz-Ferreras, R. Gomez-Garcia, and C. Z. Li, "FMCW radar fall detection based on ISAR processing utilizing the properties of RCS, range, and Doppler," in *IEEE MTT-S Int. Microw. Symp. Dig.*, May 2016, pp. 1–3.

[21] J. D. Bryan, J. Kwon, N. Lee, and Y. Kim, "Application of ultra-wide band radar for classification of human activities," *IET Radar, Sonar Navigat.*, vol. 6, no. 3, pp. 172–179, Mar. 2012.

[22] Z. Gu *et al.*, "Remote blind motion separation using a single-tone SIMO Doppler radar sensor," *IEEE Trans. Geosci. Remote Sens.*, vol. 57, no. 1, pp. 462–472, Jan. 2019.

[23] C. W. Ding *et al.*, "Non-contact human motion recognition based on UWB radar," *IEEE J. Emerg. Sel. Topics Circuits Syst.*, vol. 8, no. 2, pp. 306–315, Jun. 2018.

[24] L. Yang, G. Chen, and G. Li, "Classification of personnel targets with baggage using dual-band radar," *Remote Sens.*, vol. 9, no. 6, p. 594, Jun. 2017.

[25] Y. Li, Z. Peng, R. Pal, and C. Li, "Potential active shooter detection based on radar micro-Doppler and range-doppler analysis using artificial neural network," *IEEE Sensors J.*, vol. 19, no. 3, pp. 1052–1063, Feb. 2018.

[26] L. Vignaud, A. Ghaleb, J. L. Kernec, and J. Nicolas, "Radar high resolution range & micro-Doppler analysis of human motions," in *Proc. Int. Radar Conf. Surveill. Safer World, Radar*, Bordeaux, France, Oct. 2009, pp. 1–6.

[27] B. Jokanovic, M. Amin, and F. Ahmad, "Radar fall motion detection using deep learning," in *Proc. IEEE Radar Conf. (Radarconf)*, May 2016, pp. 446–451.

[28] Y. Kim and T. Moon, "Human detection and activity classification based on micro-Doppler signatures using deep convolutional neural networks," *IEEE Geosci. Remote Sens. Lett.*, vol. 13, no. 1, pp. 8–12, Jan. 2016.

[29] M. S. Seyfioğlu, A. M. Özbayoglu, and S. Z. Gürbüz, "Deep convolutional autoencoder for radar-based classification of similar aided and unaided human activities," *IEEE Trans. Aerosp. Electron. Syst.*, vol. 54, no. 4, pp. 1709–1723, Aug. 2018.

[30] Y. Lin, J. Le Kernec, S. Yang, F. Fioranelli, O. Romain, and Z. Zhao, "Human activity classification with radar: Optimization and noise robustness with iterative convolutional neural networks followed with random forests," *IEEE Sensors J.*, vol. 18, no. 23, pp. 9669–9681, Dec. 2018.

[31] G. Bergen, "Falls and fall injuries among adults aged ≥65 years—United States, 2014," *MMWR Morbidity Mortality Weekly Rep.*, vol. 65, no. 37, pp. 993–998, 2016.

[32] T. K. Ho, "Nearest neighbors in random subspaces," in *Proc. Joint IAPR Int. Workshops Stat. Techn. Pattern Recognit. (SPR) Struct. Syntactic Pattern Recognit. (SSPR)*, 1998, pp. 640–648.

[33] Z. Zhou, *Ensemble Methods: Foundations and Algorithms*. London, U.K.: Chapman & Hall, 2012.

[34] G. Wang, C. Gu, T. Inoue, and C. Li, "A hybrid FMCW-interferometry radar for indoor precise positioning and versatile life activity monitoring," *IEEE Trans. Microw. Theory Techn.*, vol. 62, no. 11, pp. 2812–2822, Nov. 2014.

Chuanwei Ding (S'17) received the B.S. degree in electronic and information engineering from the Nanjing University of Science and Technology, Nanjing, China, in 2014, where he is currently pursuing the Ph.D. degree.

He is currently with the Department of Electrical and Computer Engineering, Texas Tech University, Lubbock, TX, USA, as a Visiting Scholar. His research interests include biomedical applications of microwave technology and radar signal processing.

Hong Hong (M'10) received the Ph.D. degree in electrical engineering from Nanjing University, Nanjing, China, in 2010.

He is currently an Associate Professor with the School of Electronic and Optical Engineering, Nanjing University of Science and Technology, Nanjing. His research interests include biomedical applications of microwave technology, audio signal processing, and radar signal processing. In 2014, he was a Visiting Scholar with the Institute of Biomedical Engineering and Technology, Sydney University, Sydney, NSW, Australia.

Dr. Hong has served as a Steering Committee Member and a TPC Member. He also serves as a member of the IEEE MTT-S Biological Effect and Medical Applications of RF and Microwave (MTT-10). He has also served as the Session Chair for IMBioC, IWS, and ACES. He is a Guest Editor of the IEEE JOURNAL OF ELECTROMAGNETICS, RF AND MICROWAVES IN MEDICINE AND BIOLOGY.

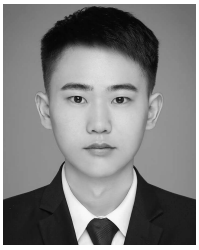

Yu Zou (S'18) received the B.S. degree in electronic and information engineering from the Nanjing University of Science and Technology, Nanjing, China, in 2016, where he is currently pursuing the master's degree with the School of Electronic and Optical Engineering.

His research interests include radar signal processing and target detection.

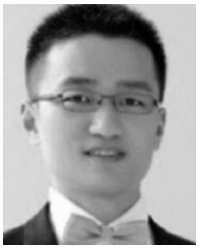

Hui Chu was born in Nantong, China, in 1985. He received the B.S. degree in electrical and information engineering and the Ph.D. degree from the Nanjing University of Science and Technology, Nanjing, China, in 2007 and 2012, respectively.

From 2013 to 2017, he was a Lecturer with Nantong University, Nantong. He is currently an Associate Professor with the School of Electronic and Optical Engineering, Nanjing University of Science and Technology. He has authored or coauthored over 20 international journal or conference papers. He holds two Chinese patents. His research interests include millimeter-wave antennas, filters, and filtering antennas based on LTCC and micromachined technologies.

Xiaohua Zhu (M'07) received the Ph.D. degree in communication and information system from the Nanjing University of Science and Technology, Nanjing, China, in 2002.

He is currently a Professor with the School of Electronic and Optical Engineering, Nanjing University of Science and Technology, where he is also the Director of the Radar and High-speed Digital Signal Processing Laboratory. He has authored or coauthored four books and more than 100 papers. He has submitted 18 patent applications. His research interests include radar systems, radar signal theory, and digital signal processing.

Dr. Zhu was a ten-time recipient of the Ministerial and Provincial-Level Science and Technology Award.

Francesco Fioranelli (M'15) received the Ph.D. degree in electronic engineering from Durham University, Durham, U.K., in 2014.

He has been an Assistant Professor with the University of Glasgow, Glasgow, U.K., since 2016. He was a Research Associate with University College London, London, U.K., prior to joining the University of Glasgow. He has coauthored more than 60 papers in international conference proceedings and academic journals on various applications of radar systems. His research interests include multistatic and distributed radar sensing, application of machine learning to radar data for classification in healthcare and security, characterization of radar signatures of vehicles and UAVs, wind farms, and sea clutter.

Julien Le Kernec (SM'17) received the B.Eng. and M.Eng. degrees in electronic engineering from the Cork Institute of Technology, Cork, Ireland, in 2004 and 2006, respectively, and the Ph.D. degree in electronic engineering from University Pierre and Marie Curie, Paris, France, in 2011.

He is currently a Lecturer with the School of Engineering, University of Glasgow, Glasgow, U.K. He is also a Lecturer with the University of Electronic Science and Technology of China, Chengdu, China, and an Adjunct Associate Professor with the ETIS Lab, University of Cergy-Pontoise, Cergy, France. His research interests include radar system design, software-defined radio/radar, signal processing, and health applications.

Changzhi Li (S'06–M'09–SM'13) received the B.S. degree in electrical engineering from Zhejiang University, Hangzhou, China, in 2004, and the Ph.D. degree in electrical engineering from the University of Florida, Gainesville, FL, USA, in 2009.

From 2007 to 2009, he was first with Alereon Inc., Ausitn, TX, USA, and then with Coherent Logix Inc., Austin, TX, USA, where he was involved in ultrawideband (UWB) transceivers and software-defined radio, respectively. In 2009, he joined Texas Tech University, Lubbock, TX, USA, as an Assistant Professor, and became an Associate Professor in 2014. His research interests include biomedical applications of microwave technology, wireless sensors, and RF/analog circuits.

Dr. Li was a recipient of the IEEE Microwave Theory and Techniques Society (MTT-S) Outstanding Young Engineer Award, the IEEE Sensors Council Early Career Technical Achievement Award, the ASEE Frederick Emmons Terman Award, the IEEE-HKN Outstanding Young Professional Award, the NSF Faculty Early CAREER Award, and the IEEE MTT-S Graduate Fellowship Award. He is an Associate Editor of the IEEE TRANSACTIONS ON MICROWAVE THEORY AND TECHNIQUES, the IEEE TRANSACTIONS ON CIRCUITS AND SYSTEMS I, and the IEEE JOURNAL OF ELECTROMAGNETICS, RF AND MICROWAVES IN MEDICINE AND BIOLOGY. He served as an Associate Editor of the IEEE TRANSACTIONS ON CIRCUITS AND SYSTEMS II from 2014 to 2015. He served as a TPC Co-Chair for the IEEE MTT-S International Microwave Biomedical Conference from 2018 to 2019 and the IEEE Wireless and Microwave Technology Conference from 2012 to 2013.